



A highly sensitive electrochemical sensor by growing Ag nanoparticles on the surface of PPy@PEDOT:PSS film for detecting sodium hydroxymethanesulfinate molecules

Tianwen Xu ^{a,b}, Li Yang ^{a,b}, Xin Zhang ^b, Guo Lu ^b, Zhongchen Bai ^{a,b,*}

^a College of Medicine, Guizhou University, Guiyang City 550025, China

^b Guizhou Province Key Lab. for Photoelectric Technology and Application, Guizhou University, Guiyang City 550025, China

ARTICLE INFO

Keywords:

Electrochemical sensor
Sodium hydroxymethanesulfinate
Ag nanoparticles (AgNPs)
Polypyrrole@Poly(3,4-ethylenedioxythiophene)-poly(styrenesulfonate)
Differential pulse voltammetry
Milk matrix
Raman spectroscopy

ABSTRACT

A high-sensitivity electrochemical sensor was fabricated via in situ growth of Ag nanoparticles (AgNPs) on the surface of a polypyrrole@poly(3,4-ethylenedioxythiophene):polystyrene sulfonic acid (PPy@PEDOT:PSS) film for detecting sodium hydroxymethanesulfinate (SHF) molecules in milk and rice flour samples. The sensor fabrication process involved randomly decorating Ag seed points on the porous PPy@PEDOT:PSS film via a chemical reduction process using a AgNO₃ solution. Next, AgNPs were anchored on the PPy@PEDOT:PSS film surface using an electrochemical deposition method to prepare a sensor electrode. Under optimal conditions, the sensor exhibits a good linear relation within a range of 1–130 ng/mL for real milk and rice flour samples and its limit-of-detection values were up to 0.58 and 0.29 ng/mL, respectively. Additionally, Raman spectroscopy was used to identify the byproducts of the chemical reaction, such as formaldehyde. This AgNP/PPy@PEDOT:PSS film-based electrochemical sensor offers a simple and rapid method for detecting SHF molecules in food products.

Introduction

Sodium hydroxymethanesulfinate (NaHOCH₂SO₂·2H₂O, SHF) was once used as an excellent decoloring reagent for various organic compounds in industrial bleaching applications. It has been also added to milk and flour to enhance their whiteness. However, SHF is harmful to the human body and results in hepatotoxicity and nephrotoxicity when ingested through the skin, mouth, and nose. Therefore, its use in food is prohibited. Unfortunately, some dishonest merchants still add SHF to foods such as rice flour, noodles, and steamed bread to improve their resilience and extend their shelf life (Yuan, Xiang, Yu, & Xu, 2011). Consequently, there is a need to develop a simple, fast, and accurate detection technology for identifying and quantifying SHF in food. Primary SHF detection techniques include ion chromatography (Dovrou, Lim, Canagaratna, Kroll, Worsnop, & Keutsch, 2019), high-separation liquid chromatography (Jing et al., 2018; Nesměrāk et al., 2019), spectrophotometry (Abedalwafa et al., 2020), and electrochemical (EC) sensing (Wu et al., 2018). Although chromatography methods exhibit high accuracy and sensitivity, they require sample derivatization during sample processing. Furthermore, spectrophotometric techniques, such

as the photocolometric method, require a complicated chemical reaction. To address these drawbacks, EC analysis has attracted attention in the biosensor field owing to its easy operation, excellent sensitivity, versatility, miniaturization prospect, and the ability to improve selectivity and specificity by modifying the electrode surface (Dong, Ryu, & Lei, 2021; Li et al., 2019; Mohan et al., 2020; Noori, Mortensen, & Geto, 2020; Qian, Durairaj, Prins, Chen, & Bioelectronics, 2021). Furthermore, the electrochemical oxidation process of SHF can be monitored in situ and in real-time by integrating with Raman technology.

Nanomaterials have garnered considerable interest in the field of EC sensors and surface-enhanced Raman scattering of molecules as they serve as a bridge between analytes and electrochemical electrodes (Liu et al., 2018; Manikandan, Adhikari, & Chen, 2018; Wu et al., 2020; Xiao, Huang, Wang, Meng, & Yang, 2020). EC sensors prepared using nanomaterials have found widespread use in detecting compounds in food (Bavandpour et al., 2016; Shahmiri, Bahari, Karimi-Maleh, Hosseinzadeh, Mirnia, & Chemical, 2013; Yola et al., 2015). Ag nanoparticles (AgNPs) are a classic example of a linker between analytes and electrodes and are widely employed owing to their low toxicity, biocompatibility, sustainable electrochemical catalytic activity, and high

* Corresponding author.

E-mail address: zcbai@gzu.edu.cn (Z. Bai).

<https://doi.org/10.1016/j.fochx.2023.100701>

Received 11 December 2022; Received in revised form 26 April 2023; Accepted 30 April 2023

Available online 8 May 2023

2590-1575/© 2023 The Author(s). Published by Elsevier Ltd. This is an open access article under the CC BY-NC-ND license (<http://creativecommons.org/licenses/by-nc-nd/4.0/>).

surface plasmon resonance (Kaur et al., 2022; Loiseau et al., 2019; Song et al., 2018; Tufa et al., 2018; Zhu et al., 2019). However, rapid aggregation caused by AgNP interactions can considerably reduce the sensitivity of a sensor. To prevent their aggregation, AgNPs are anchored on the surfaces of various substrates. For instance, Wan and Zheng used AgNPs decorated on carbon nanotubes to detect nitrite (Wan, Zheng, Wan, Yin, & Song, 2017). Jodan and Wantala fabricated an EC sensor based on AgNPs loaded on the surface of an alizarin yellow polymer for detecting thiourea, an ecological pollutant (Jodan et al., 2020). Furthermore, Fatemeh synthesized a sensor electrode-based AgNP-polyaniline nanocomposite to detect the drug 5-fluorouracil (Zahed et al., 2018). However, the aforementioned methods have limitations, such as being labor-intensive and expensive as well as having poor reproducibility and low sensitivity, making them unsuitable for widespread practical applications.

Polypyrrole (PPy), a typical intrinsic polymer, can be prepared as a conductive film using the anodic electrodeposition method (Wang et al., 2018; Zhang et al., 2017); moreover, its electropolymerization process is convenient efficient. Additionally, PPy films exhibit surface uniformity and good biocompatibility. Furthermore, the abundant pore distribution of PPy films allows for easy absorption of other organic molecules, creating active sites for reducing ions and organic molecules. Metals nanostructures (such as Ag, Pt, Cu, and Au) can also be effectively immobilized on the surface of PPy films, making them excellent materials for preparing electrochemical sensor electrodes (Maruno, 2019; Wang et al., 2022).

This study proposes a highly sensitive electrochemical sensor for detecting SHF in milk and rice flour samples. First, we used an electrochemical anodic polymerization method to prepare PPy@PEDOT:PSS (PEDOT:PSS: poly(3,4-ethylenedioxythiophene): polystyrene sulfonic acid) films on a steel sheet (SLT) plane. Subsequently, AgNPs were anchored to the PPy@PEDOT:PSS film surface using a chemical reduction method and electrochemical cathode deposition method to fabricate an EC sensor electrode. In comparison with other preparation methods for EC sensor electrodes, the proposed EC method did not require a complex experimental procedure and expensive equipment. Consequently, the EC sensor we proposed can be easily implemented on an industrial scale for detecting hazardous substances in food owing to its high sensitivity and cost-effective manufacturing process.

Experiments

2.1. Materials and reagents

Sodium hydroxymethanesulfinate molecules (98%, Aladdin Reagent Co., LTD.) were used as detection molecules. A steel sheet (SLT) with dimensions of $100 \times 100 \times 0.02 \text{ mm}^3$ was purchased from Shenzhen Jinchenyu Co., LTD. Absolute ethanol ($\text{C}_2\text{H}_5\text{OH}$, %99), PEDOT:PSS (ASC, 95%), PPy (ASC, 98%), ascorbic acid (ASA) powder (ASC, 99%), citric acid powder (ASC, 99%), Ag nitrate powder (AgNO_3 , 99%), $\text{K}_3\text{Fe}(\text{CN})_6$ and $\text{K}_4\text{Fe}(\text{CN})_6$ (ASC, 99%), KCl (ASC, 99%), sodium sulfite (ASC, 99%), and 0.2 M phosphate buffer solution (PBS) (ASC, 99%) were all sourced from Aladdin Co. Ltd. (Shanghai, China). Commercial milk and rice flour were purchased from a local supermarket for subsequent real sample analyses. Deionized water was obtained from a MilliQ water purification system.

2.2. Preparation of AgNP/PPy@PEDOT:PSS/SLT electrodes

2.2.1. Preparation of PPy@PEDOT:PSS films

PPy@PEDOT:PSS films were prepared in four steps: (1) A $100 \text{ mm} \times 100 \text{ mm} \times 0.02 \text{ mm}$ steel sheet (SLT) was rinsed with absolute ethanol for 5 min to remove surface dust. The sheets were then placed in an ultrasonic cleaning machine to remove any remaining contaminants. (2) A 20-mL PPy@PEDOT:PSS electrolyte solution was prepared by mixing 0.7-mL PEDOT:PSS and 0.7-mL pyrrole. (3) The Pt electrode was used as

a counter electrode (cathode), whereas the SLT plate was used as the working electrode (anode). Subsequently, a PPy@PEDOT:PSS film was electrodeposited on the working electrode in the 20-mL PPy@PEDOT:PSS electrolyte solution using an electrochemical workstation (Autolab PGSTAT302N) at a constant voltage of 3 V. (4) After electropolymerization for 30 min, the working electrode was rinsed with deionized water for 4 min to remove the unpolymerized electrolyte and other surface residues.

2.2.2. Preparing AgNPs on the surface of PPy@PEDOT:PSS films

The preparation procedure of AgNPs on the PPy@PEDOT:PSS films consisted of the following steps: (1) The PPy@PEDOT:PSS films were pretreated by immersing them in 20 mL 0.02 M ASA solution for 24 h. The films were then washed four times with deionized water to remove the residual solution. (2) The pretreated PPy@PEDOT:PSS films were immersed in a 20-mL 0.06-M AgNO_3 solution for 40 s to self-assemble Ag seed points on the film. The film was then removed, rinsed with deionized water, and allowed to air dry naturally. (3) The PPy@PEDOT:PSS films with Ag seed points served as working electrodes (cathode). A current of 0.23 mA/cm^2 was applied on the electrodes to grow dense AgNPs in an AgNO_3 -citric acid mixture solution, prepared by mixing 0.36 g of citric acid, 0.04 g of AgNO_3 powders, and 20 mL of deionized water. After electrodeposition for 40 min, the AgNPs/PPy@PEDOT:PSS layered structure electrode was removed and left to air dry.

2.2.3. Preparation of SHF sample solution

To prepare SHF solution, 1 mg of SHF powder was dissolved in deionized water, resulting in a $10\text{-}\mu\text{g/mL}$ solution. This solution was then diluted into a 20-mL detection solution of different concentrations (130, 120, 110, 100, 80, 60, 40, 20, 10, and 1 ng/mL).

2.2.4. Preparation of real samples

The ability of the AgNP/PPy@PEDOT:PSS/SLT film to detect SHF in milk and rice flour samples was evaluated through a series of processing steps: (1) A mixture of 1-mL pure milk or 1-g rice flour, 10-mL 5% $\text{C}_2\text{HCl}_3\text{O}_2$ (TCA), and 1-mL $(\text{CH}_3\text{COO})_2\text{Pb}$ was added to a centrifuge tube; (2) The sample was subjected to vortex oscillation for 1 min and then kept in an ultrasonic bath for 10 min; (3) The samples were centrifuged at 7500 rpm for 15 min; (4) The supernatant was collected using a $0.45\text{-}\mu\text{m}$ membrane filter after centrifugation; (5) Subsequently, 1 mL of the sample supernatant was diluted to 10 mL with a sodium PBS (0.2 M and pH = 7.6). (6) SHF solutions of different concentrations (130, 120, 110, 100, 80, 60, 40, 20, 10, and 1 ng/mL) were added to the diluted sample solution for EC detection. Furthermore, the milk and rice flour sample solutions were spiked with known SHF standard concentrations and analyzed for EC spike recovery using the standard addition method in triplicate ($n = 3$).

2.3. Characterization

Cyclic voltammetry (CV) spectra, differential pulse voltammetry (DPV), and electrochemical impedance spectroscopy (EIS) spectra were measured using an Autolab PGSTAT302N electrochemical workstation. A three-electrode system was used to evaluate the performance of the AgNPs/PPy@PEDOT:PSS electrode. The working, counter, and reference electrodes were an AgNPs/PPy@PEDOT:PSS/SLT layered film, a Pt wire, and an Ag/AgCl saturating electrode, respectively. A scanning electron microscope, energy-dispersive spectrometer (SU8100, Hitachi, Japan), and X-ray diffractometer (D8 Advance, Bruker, Germany) were used to analyze the morphologies and elemental composition of AgNPs films. Furthermore, a Fourier transform infrared spectrometer (V-70 + H1000, Bruker, Germany) was used to examine the molecular binding properties of PPy@PEDOT:PSS. A microRaman spectrometer (SR-500I-B1, Andor, North Ireland) equipped with a 633-nm continuous laser (Solna, Cobolt 08-NLD) and connected to a material microscope was employed for measuring in situ Raman information of the electrode

surface in a three dimensional (3D)-printed electrochemical Raman cell.

2.4. Electrochemical measurement of samples

This study used the DPV method to detect SHF in the presence of 0.2-M PBS with a pH of 7.6 as a supporting electrolyte. Additionally, CV and EIS techniques were used to obtain information from the electrode surface. The voltage range of CV voltammograms was set between -0.5 V and $+0.90$ V in a mixture solution of $[\text{Fe}(\text{CN})_6]^{3-/4-}$ and 0.1-M KCl as a redox probe. Furthermore, EIS curves were obtained by setting the frequency range of EIS spectra between 0.01 Hz and 100 kHz, and the EIS solution comprised 1.0-mM $[\text{Fe}(\text{CN})_6]^{3-/4-}$ and 0.1-M KCl. Additionally, the potential range, increment potential, pulse width, and pulse interval of the DPV were set at 0–1.00 V, 0.010 V, 0.05 s, and 0.5 s, respectively.

2.5. In situ surface-enhanced Raman scattering measurement

In Fig. 1, the CV method, an electrochemical technique, was integrated with surface-enhanced Raman scattering to create an electrochemical sensor for detecting SHF using a 3D-printed electrochemical Raman cell. The CV method was used to measure the electrochemical oxidation process of SHF. Simultaneously, Raman spectra of the electrochemical oxidation process of SHF were recorded. Herein, a 3D-printed electrochemical Raman cell was used for the electrochemical Raman spectroscopy measurement. CV measurement parameters comprised three cyclic potentials of $+1.1$ and 0 V, starting at 0.01 V in a positive direction at 0.06 V/s. The experimental measurements were conducted in a 0.2-M PBS electrolyte solution (pH = 7.6) containing 100-ng/mL SHF molecules.

Results and discussions

3.1. Surface analysis of AgNPs/PPy@PEDOT: PSS electrode

Fig. 2 shows the surface topographies of the porous structure of the PPy@PEDOT:PSS film and AgNPs on the PPy@PEDOT:PSS film

surface. The appearance of AgNPs was similar to that of a ball with a flower edge. The diameter of the AgNPs was approximately 90–100 nm. Furthermore, the energy-dispersive X-ray spectroscopy shows the AgNPs/PPy@PEDOT:PSS electrode were mainly composed of Ag elements (Fig. 3A). The X-ray diffraction spectra for AgNPs exhibits four peaks at 38.1° , 44° , 64.5° , and 77.6° , corresponding to Ag (111), Ag (200), Ag (220), and Ag (311), respectively, according to the JCPDS04-0783 card (Fig. 3B).

The FTIR spectrum of pristine PEDOT:PSS FTIR exhibited absorption peaks at 828 and 1159 cm^{-1} (Fig. 3C), ascribed to the C–S stretching and S=O stretching band of PEDOT:PSS (Xia et al., 2010). The peaks at 1493 cm^{-1} were assigned to the C–C band stretching vibrations of the PEDOT:PSS thiophene ring (Yue et al., 2012). Furthermore, a peak at 3334 cm^{-1} indicated the presence of hydroxyl groups in PEDOT:PSS (Xiong et al., 2021). Moreover, PPy@PEDOT:PSS exhibited an additional peak at 2840 cm^{-1} compared with PEDOT:PSS, which was attributed to the aromatic ring vibrations of the PPy (Pasupuleti et al., 2020; Ren et al., 2021). Thus, the PPy@PEDOT:PSS film was successfully polymerized on the SLT surface.

3.2. Electrochemical properties of AgNPs/PPy@PEDOT: PSS/SLT film

The interfacial electron kinetics of the electrode surface were studied via CV measurements. Fig. 4A shows the CV curves of the bare SLT, PPy@PEDOT:PSS/SLT, AgNPs/SLT, and AgNPs/PPy@PEDOT:PSS/SLT in 1.0-mM $[\text{Fe}(\text{CN})_6]^{3-/4-}$ and 0.1-mM KCl redox probe. A prominent redox peak was observed for the bare SLT at 0.2 V. When the SLT was modified with PPy@PEDOT:PSS, the redox peak increased in intensity, indicating that PPy@PEDOT:PSS could enhance the electrical conductivity. Furthermore, after anchoring AgNPs on the SLT, its peak current further increased compared with those of the bare SLT and PPy@PEDOT:PSS/SLT owing to the strong electrical conductivity of AgNPs. For the AgNPs/PPy@PEDOT:PSS/SLT electrode, the redox peak substantially increased in intensity, demonstrating that the electron transfer rate was considerably accelerated, thereby boosting the electrochemical activity through the synergistic effect between AgNPs and PPy@PEDOT:PSS. Additionally, the active electrode area at various modification

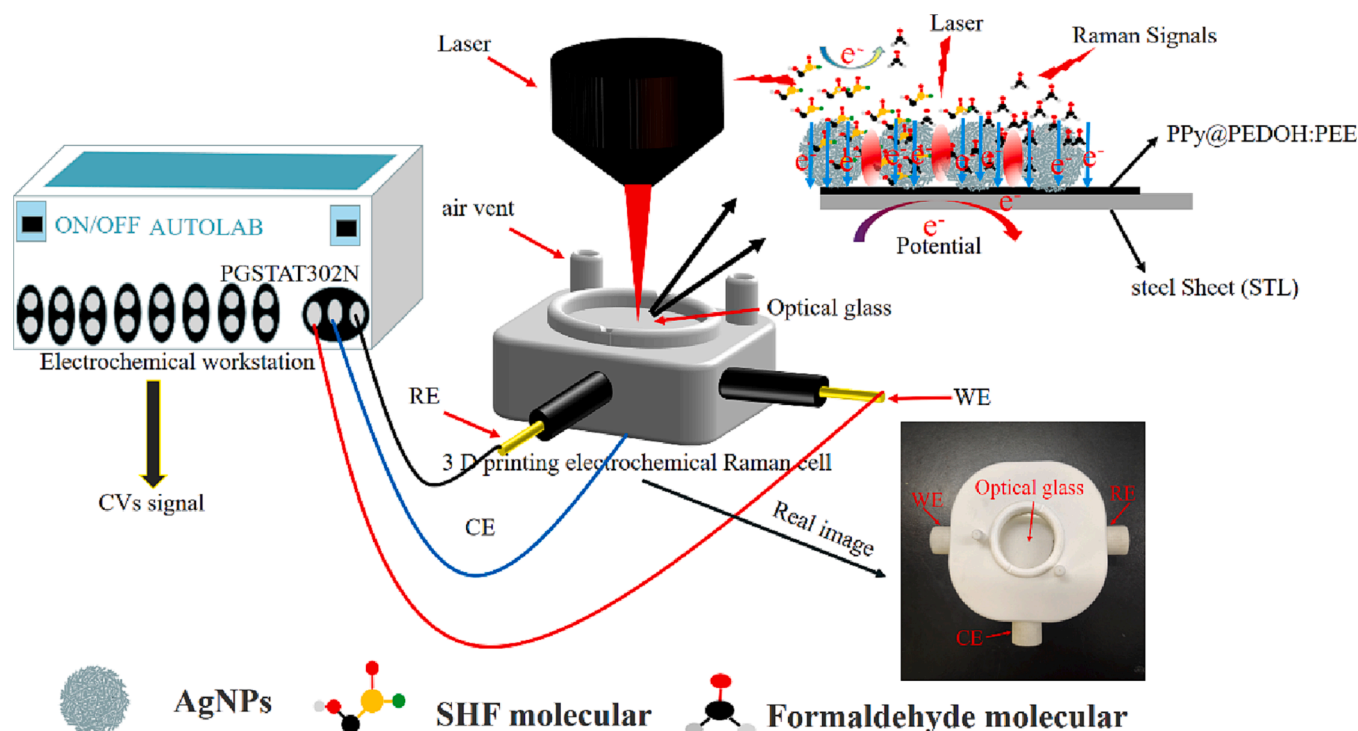


Fig. 1. Schematic map of in situ electrochemical Raman signal measurement system.

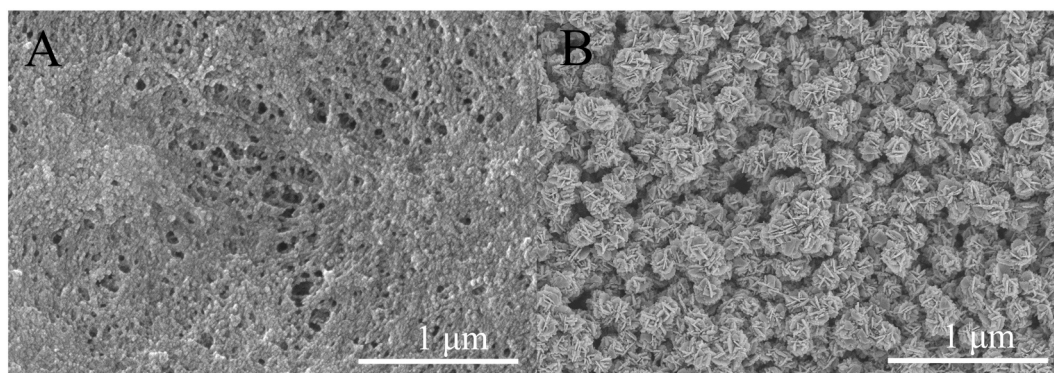


Fig. 2. Scanning electron microscopy images of (A) PPy@PEDOT:PSS/SLT film surface and (B) AgNPs/PPy@PEDOT:PSS/SLT electrode.

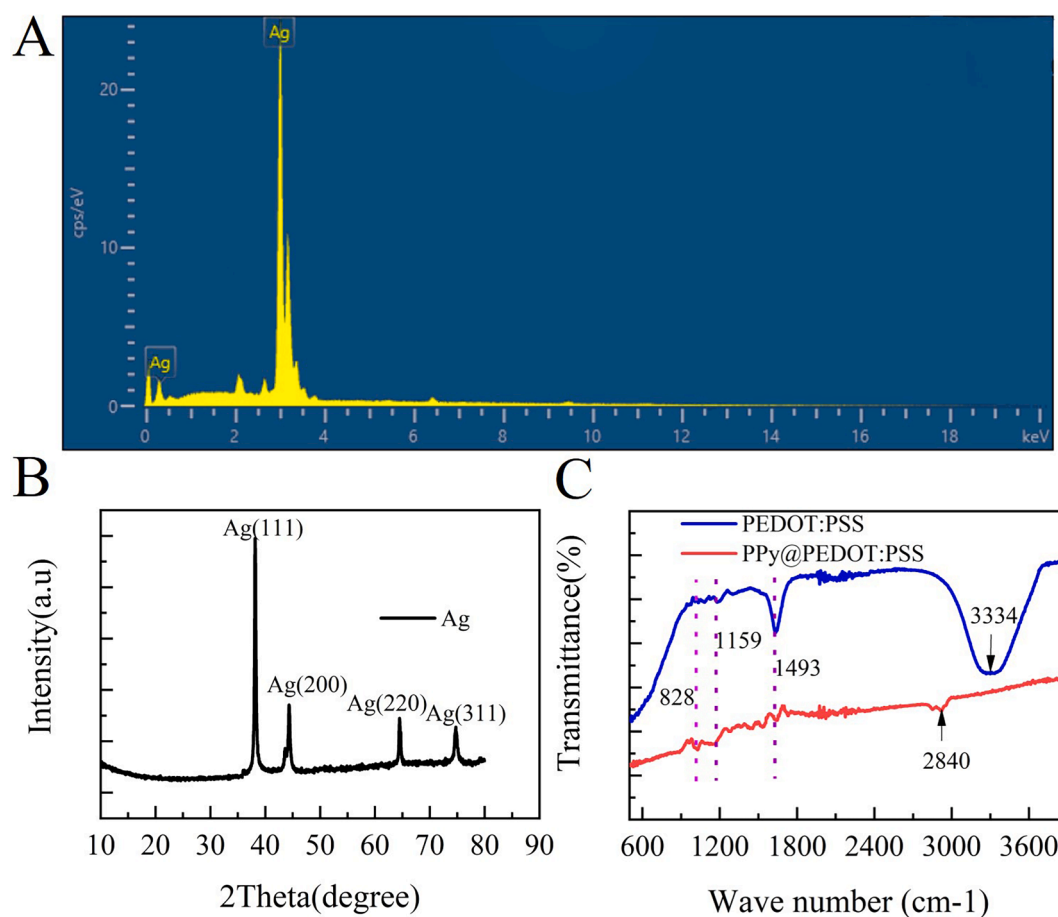


Fig. 3. (A) Energy-dispersive X-ray spectroscopy map of AgNPs; (B) X-ray diffraction pattern of AgNPs; (C) Fourier transform infrared spectra of PEDOT:PSS and PPy@PEDOT:PSS.

stages was calculated using the Randles–Sevcik equation, as shown in equation (1) (Hatamluyi and Es' hagh, 2018):

$$I = (2.69 \times 10^5) n^{3/2} A_0 D_0^{1/2} C_0 \nu^{1/2} \quad (1)$$

where I denotes an anodic peak current, D_0 denotes the diffusion coefficient, $D_0 = 7.6 \times 10^{-6} \text{ cm}^2 \text{ s}^{-1}$, ν denotes the scan rate, A_0 denotes the surface area of the electrode, and C_0 denotes the concentration of the $[\text{Fe}(\text{CN})_6]^{3-/4-}$ solution ($C_0 = 1.0 \text{ mM}$); the electron transfer number n is set as 1. In this study, the surface areas of the SLT, PPy@PEDOT:PSS/SLT, AgNPs/SLT, and AgNPs/PPy@PEDOT:PSS/SLT were calculated to be 0.157, 0.184, 0.201, and 0.270 cm^2 , respectively. These results

showed that the AgNPs/PPy@PEDOT:PSS/SLT film electrode could increase the active surface area of the EC sensor.

The EIS curves of the SLT, PPy@PEDOT:PSS/SLT, AgNPs/SLT, AgNPs/PPy@PEDOT:PSS/SLT are shown in Fig. 4B, which comprised a semicircle and straight line in the high-frequency and low-frequency regions, respectively. The diameter of the semicircle shows the charge transfer resistance R_{ct} , and a slope of 1 for the straight line represents an ideal capacitive behavior. The SLT exhibited the largest semicircle diameter owing to its poor conductivity, whereas the AgNPs/PPy@PEDOT:PSS/SLT film exhibited the smallest diameter owing to its strong conductivity (Fig. 4B). These results are consistent with those shown in Fig. 2A. Thus, the electron transfer rate of the PPy@PEDOT:PSS/SLT

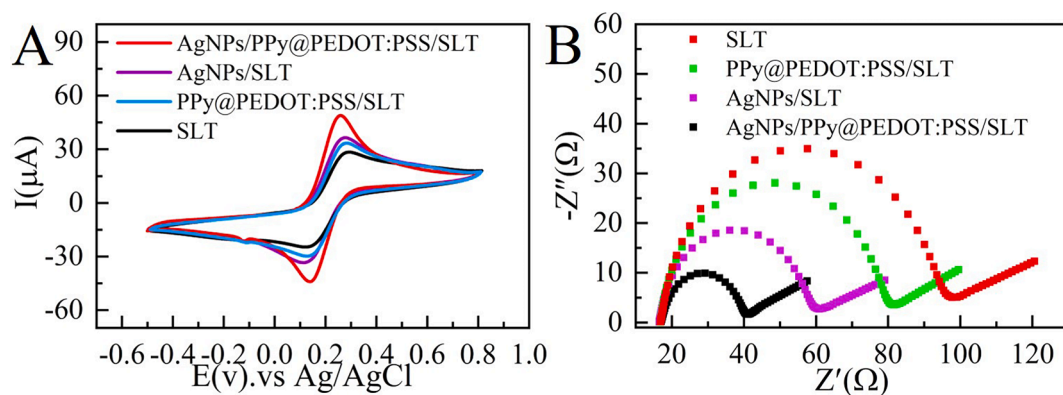


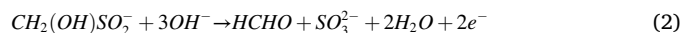
Fig. 4. (A) Cyclic voltammograms curves and (B) EIS spectra of SLT, PPy@PEDOT: PSS/SLT, AgNPs/SLT, AgNPs/PPy@PEDOT: PSS/SLT in a mixture solution of 1.0 mM $K_3Fe(CN)_6/K_4Fe(CN)_6$ and 0.1 M KCl.

film was increased by anchoring AgNPs on the surface of PPy@PEDOT: PSS/SLT (AgNP/PPy@PEDOT:PSS/SLT film) to enhance its electrochemical performance.

3.3. In situ electrochemical measurement integrating with a 3D-printed electrochemical Raman cell for detecting SHF on AgNPs/PPy@PEDOT: PSS/SLT electrodes

CV curves and Raman spectra were simultaneously measured to obtain SHF EC oxidation information (20 ng/mL) using the AgNPs/PPy@PEDOT:PSS/SLT electrode in 0.2-M PBS (pH = 7.6) supporting electrolytes (Fig. 5A and 5B). The measurement scheme is shown in Fig. 1. In Fig. 5B, the peaks observed at 2910 and 1055 cm^{-1} represent the Raman characteristic peaks of SHF under open-circuit voltage, corresponding to the $-CH_2-$ stretching vibration and S=O symmetric

stretching vibration of SHF, respectively (Wang et al., 2020; Wang, Jiang, Zhang, & Bai, 2021). Additionally, the oxidation peak of SHF was observed at 0.4–0.8 V (Fig. 5A). Furthermore, the Raman spectra changed substantially compared with the open-circuit voltage in Fig. 5B, with four peaks appearing at 595, 1119, 1535, 3086 cm^{-1} . This Raman spectroscopy results were consistent with the Raman signal obtained for formaldehyde (Lebrun et al., 2003). As SHF was continuously oxidized and formaldehyde was continuously generated, the Raman peak intensity of SHF continued to decrease and the Raman peak intensity of formaldehyde continued to increase. The electrochemical oxidation process of SHF at the AgNPs/PPy@PEDOT: PSS/SLT electrode can be expressed by equation (2).



Furthermore, Fig. 5C shows the CV curves of 20-ng/mL SHF in 0.2-M

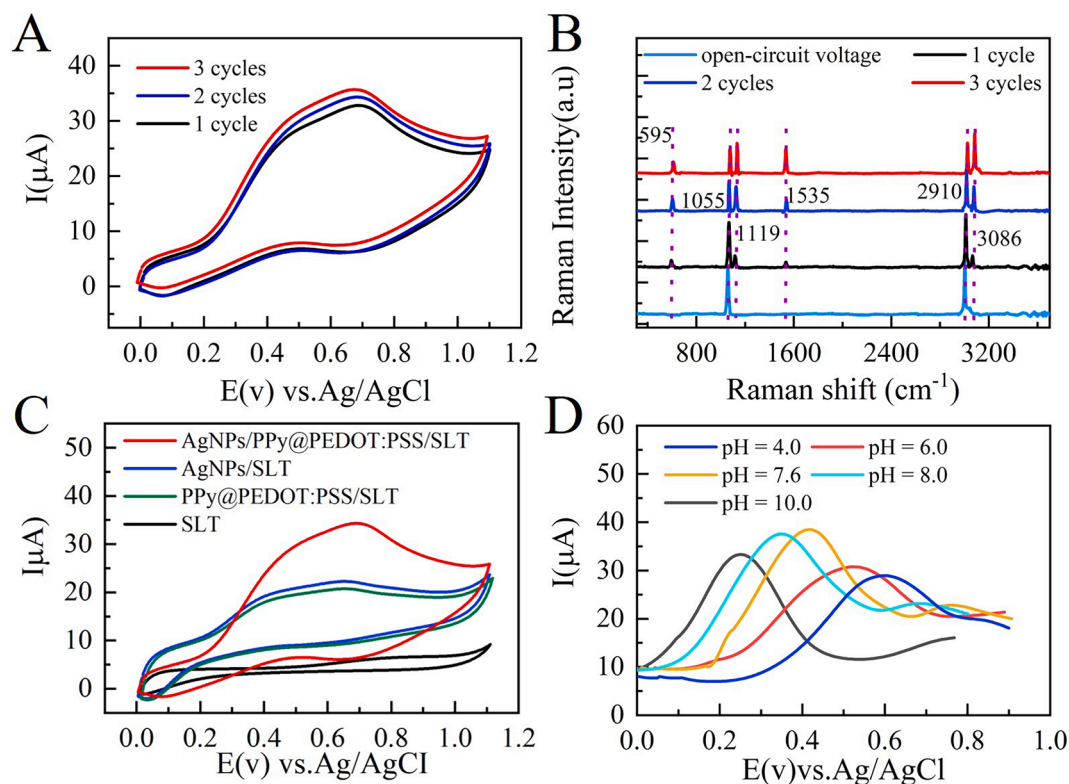


Fig. 5. (A) Cyclic voltammetry (CV) curves of 20-ng/mL SHF in the 0.2-M PBS support electrolytes (pH = 7.6) on AgNPs/PPy@PEDOT: PSS/SLT; (B) Raman signal during the CV measurement; (C) CV curves of 20-ng/mL SHF in 0.2-M PBS (pH = 7.6) at bare SLT, PPy@PEDOT: PSS/SLT, AgNPs/SLT, AgNPs/PPy@PEDOT: PSS/SLT; (D) DPVs of 20 ng/mL SHF in the pH range of 4.0–10.0 at AgNPs/PPy@PEDOT: PSS/SLT.

PBS (pH = 7.6) on the bare SLT, PPy@PEDOT: PSS/SLT, AgNPs/SLT, and AgNPs/PPy@PEDOT:PSS/SLT. AgNP/PPy@PEDOT:PSS/SLT electrode exhibits a more distinct current response to SHF compared with other modified electrodes. Thus, the AgNPs/PPy@PEDOT:PSS/SLT electrode was selected for SHF detection.

Fig. 5D shows the graph of the pH response vs. the DPV in 20-ng/mL SHF solutions for pH values from 4.0 to 10.0. The oxidation peak current gradually increased from pH = 4.0 to 7.6, reaching a maximum peak current value at pH 7.6. and then gradually decreasing for pH 7.6–10.0. Therefore, 0.2-M PBS with pH 7.6 was selected as the optimal electrolyte solution for detecting SHF.

3.4. SHF detection in PBS electrolyte solution

We selected 0.2-M PBS (pH = 7.6) as the optimal supporting electrolyte solution for detecting SHF using AgNP/PPy@PEDOT:PSS/SLT electrodes; the detection results are shown in Fig. 6A. Fig. 6A shows that the DPV current intensity increased with increasing SHF concentration in the 0.2-M PBS supporting electrolyte solution (pH = 7.6). Furthermore, Fig. 6B reveals that a linear relationship emerged between the SHF concentration and DPV current response intensity (relative to the background current measured in the PBS electrolyte solution) with increasing SHF concentration from 20 ng/mL to 130 ng/mL. The linear equation is given by equation (3):

$$I(\mu\text{A}) = 1.479 \cdot C + 13.191, R^2 = 0.9959 \quad (3)$$

According to equation (3), the slope of the equation was 1.479, indicating that the AgNP/PPy@PEDOT:PSS/SLT sensor electrode exhibited a high linear response when detecting low concentrations of SHF. Furthermore, the limit of detection (LOD) was 0.06 ng/mL (equal to 0.389 nmol/L) based on the $3S_b/m$. (S_b is the standard deviation of the blank in six experiments, and m is the slope of the linear equation curve).

3.5. Analysis of real samples

Furthermore, the ability of the AgNP/PPy@PEDOT:PSS/SLT sensor electrode to analyze SHF molecules in real samples environments was investigated. The electrochemical oxidation behavior of SHF in real milk and rice flour samples was investigated using the CV method and Raman spectroscopy. As shown in Fig. 7A, the CV curves of SHF in milk and rice flour were generally consistent with the CV curve of SHF in the PBS electrolyte solution. During the CV measurement process, the Raman spectra shown in Fig. 7B, which exhibited the Raman characteristic peaks of SHF and its oxidation products in PBS solution as well as in milk and rice flour samples, were consistent with the CV results shown in Fig. 5A. Meanwhile, the other Raman peaks were observed for SHF and its electrochemical oxidation products in the range of 1550–2890 cm^{-1}

due to the addition the $\text{C}_2\text{HCl}_3\text{O}_2(\text{TCA})$ and $(\text{CH}_3\text{COO})_2\text{Pb}$ during the processing of milk and rice flour samples. In addition, the prepared AgNP/PPy@PEDOT:PSS/SLT sensor electrode was used to detect SHF in the PBS electrolyte solution and milk and rice flour samples using the DPV detection method; the results are presented in Fig. 8A. These results indicate that the PBS electrolyte solution without the SHF molecule exhibited no current response. However, the PBS solution with 20-ng/mL SHF exhibited a unique current response, consistent with the results of the detection of SHF in the PBS solution. Furthermore, when 20-ng/mL SHF was added to the milk and rice flour samples, the DPV curve exhibited the oxidation peak of SHF and additional DPV responses. This was attributed to the incorporation of $\text{C}_2\text{HCl}_3\text{O}_2(\text{TCA})$ and $(\text{CH}_3\text{COO})_2\text{Pb}$ solution during the processing of milk and rice flour samples.

To evaluate the detection ability of the AgNPs/PPy@PEDOT:PSS/SLT sensor electrode for SHF molecules in real samples, known SHF concentrations (130, 120, 110, 100, 80, 60, 40, 20, 10, and 1 ng/mL) were introduced into the milk and rice flour samples. Subsequently, DPV measurements were performed; the results are shown in Fig. 8B and 8C. These findings demonstrate that the AgNPs/PPy@PEDOT:PSS sensor successfully detected SHF molecules at concentrations as low as 1 ng/mL (6.5 nmol/L) in both the milk and rice flour samples. Moreover, the fitting curves between the SHF concentrations in the milk and rice flour samples and their corresponding DPV current response (relative to PBS background current response) are shown in Fig. 8D. The fitting curves show that the sensor exhibited slopes of 1.42 and 1.75 for the milk and rice flour samples, respectively, indicating high sensitivity toward SHF in real samples. The LOD values for SHF in the milk and rice flour samples were calculated using $3S_b/m$ values; these values were determined to be 0.58 ng/mL (3.5 nmol/mL) and 0.29 ng/mL (0.053 ng/g \approx 2.7 nmol/mL), respectively. These LOD values indicate that the sensor could detect low SHF concentrations in real samples.

3.6. Reproducibility, stability, anti-interference, and recovery rate of AgNPs/PPy@PEDOT: PSS/SLT sensor

The reproducibility of the developed sensor was examined, as shown in Fig. S1A, B. Three sensors were fabricated using the same experimental parameters and employed to detect the same concentration of SHF in milk samples, with DPV current responses recorded for each sensor.

The current values were 134, 132.8, and 140.7 μA , with a relative standard deviation (RSD) of 3.13%, suggesting excellent reproducibility and minimal deviation among the three sensors. Using the same sensor, the SHF in the same milk sample was measured five times; resulting in DPV response currents of 132.8, 133.7, 132.5, 133.9, and 133.8 μA , with an RSD of 0.43%, confirming that the sensor has good and acceptable reproducibility to detect SHF in the real samples.

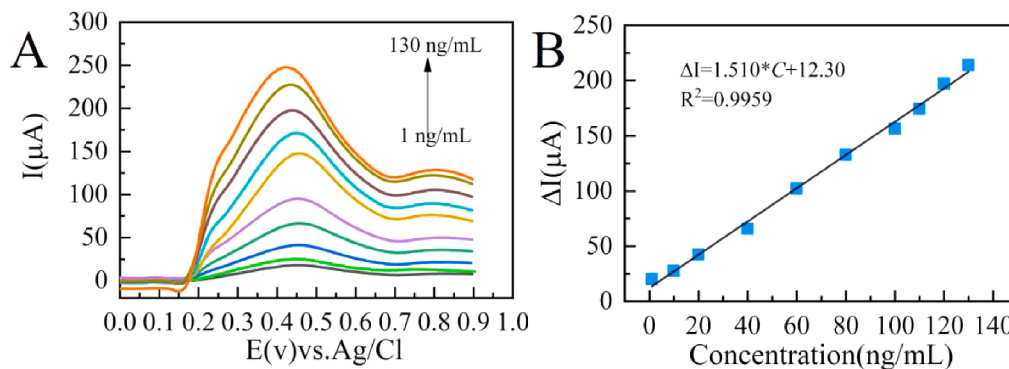


Fig. 6. (A) Differential pulse voltammetry (DPV) curves of SHF at different concentrations (1, 10, 20, 40, 60, 80, 100, 110, 120, and 130 ng/mL). (B) Curve Fitting curve between DPV response peak values and different concentrations of SHF.

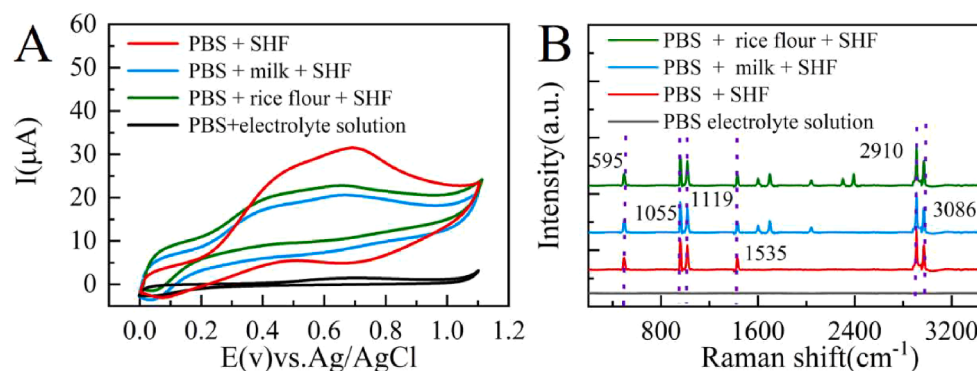


Fig. 7. (A) Cyclic voltammetry (CV) curves of the PBS electrolyte solution, and the CV curves of SHF in PBS solution and in milk and rice flour samples; (B) Raman spectra of the PBS electrolyte solution and SHF in PBS solution and in milk and rice flour samples obtained during CV measurement.

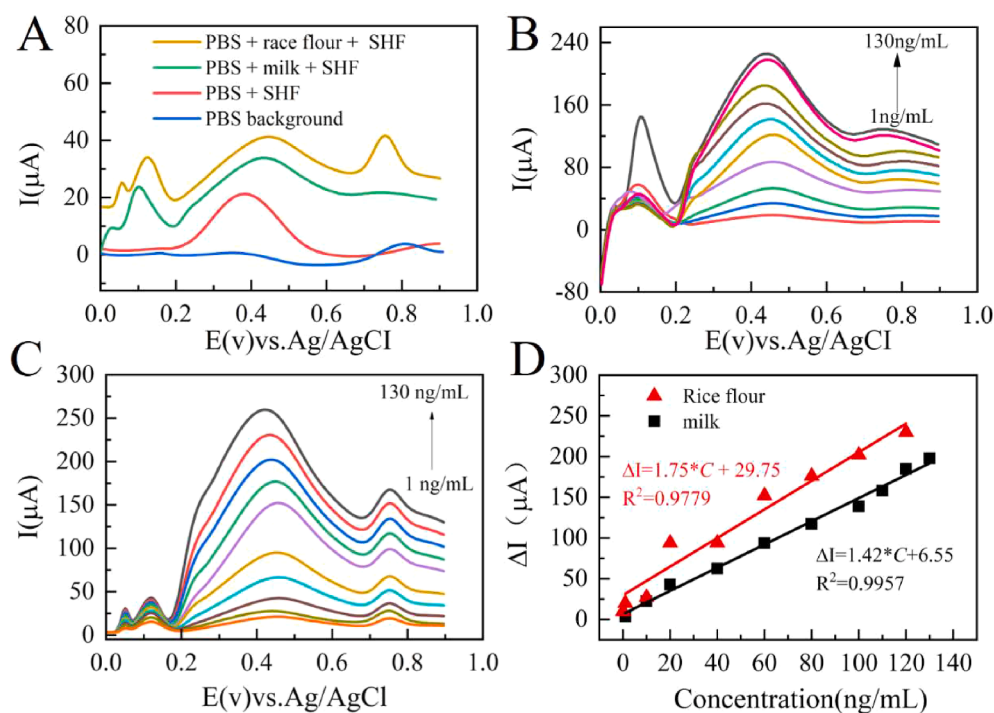


Fig. 8. (A) Differential pulse voltammetry (DPV) curves for SHF in the PBS solution and milk and rice flour samples; (B) DPV curves for different concentrations of SHF in milk samples; (C) DPV curves for different concentrations of SHF in rice flour samples; (D) Linear fitting curves between the DPV response peak currents and different concentrations of SHF in milk (black line) and rice flour (red line) samples. (For interpretation of the references to colour in this figure legend, the reader is referred to the web version of this article.)

To ensure the long-time stability of the proposed sensor, the AgNP/PPy@PEDOT:PSS/SLT electrode was stored in air for 20 days. At different storage periods between 1 and 20 days, the SLT electrode was used to detect the same SHF solution (20 ng/mL) in 0.2-M PBS (pH = 7.6) every two days starting from the first day and the current response was measured using DPV. Fig. S1C shows that the peak current response retained 80.17% of its original value until day 20, indicating good long-term stability of the fabricated sensor.

Furthermore, to verify the anti-interference properties of the sensor, ASA and oxalic were added to the milk and rice flour samples containing 20-ng/mL SHF. Fig. S1D reveals that the oxidation potentials of ASA and oxalic acid were 0.12 and 1.0 V, respectively, indicating no interference with SHF detection. To evaluate the interference of sodium sulfite from SHF decomposition in SHF detection, the AgNP/PPy@PEDOT:PSS/SLT electrode was used to detect sulfites and SHF in samples. Fig. S2 shows that the sulfite oxidation peak occurred at 1.4 V, while the detection potential of DPV ranged from 0 to 1.0 V, effectively eliminating sulfite decomposition interference. Moreover, the recovery rate of the samples was calculated. The milk and rice flour samples were spiked with known concentrations of 100.00, 200.00, and 400.00 ng/mL. Table S1 shows

that the recovery rate of spiked samples was 95.56%–100.56% and 93.2%–102.2%. This indicates that the prepared AgNP/PPy@PEDOT:PSS/SLT sensor electrode can be effectively used for detecting SHF in milk and rice flour samples.

3.7. Comparison of the sensor with other methods

Table 1 presents a comparative analysis of different SHF detection methods. The sensor developed in this study exhibits an extensive linear range and a lower LOD compared with the detection method specified by the Chinese National Standard (<https://openstd.samr.gov.cn/bzgk/gb/newGbInfo?hcno=ECD590774B7E26F29DC1D7F733A5F1BB>) for rice flour samples.

4. Conclusions

We presented a novel strategy for preparing a highly sensitive and cost-effective electrochemical sensor based on AgNP/PPy@PEDOT:PSS/SLT films with excellent selectivity for detecting SHF in milk and rice flour samples. The PPy@PEDOT:PSS film was deposited onto the bare

Table 1
Comparison of the Sensor with Other Methods.

Methods	Linear range	LOD	Ref.
Ion Chromatography and UHPLC-LTQ-Orbitrap Mass Spectrometry	9.9–143.5 $\mu\text{M}/\text{mL}$	7.3 $\mu\text{g}/\text{mL} \approx 6.1 \mu\text{M}/\text{mL}$	(Wei et al., 2020)
Electrospray Ionization-tandem Mass Spectrometry	0.6–8.6 $\mu\text{M}/\text{mL}$	10–5 M	(Chapman, Barinaga, Udseth, & Smith, 1990)
ion-pair HPLC	10–170 $\mu\text{M}/\text{mL}$	0.038 $\mu\text{M}/\text{mL}$	(Zuo & Chen, 2003)
Electrochemical detection	30–80 $\mu\text{M}/\text{mL}$	9.6 $\mu\text{M}/\text{mL}$	(Wu et al., 2018)
HPLC-MS (China National Standard Detection Method)	0.0–8.0 $\mu\text{g}/\text{g}$	0.08 $\mu\text{g}/\text{g} \approx 0.67 \mu\text{M}/\text{mL}$	https://openstd.samr.gov.cn/bzgk/gb/newGbInfo?hcno=ECD590774B7E26F29DC1D7F733A5F1BB
AgNPs/PPy@PEDOT:PSS/SLT	1–130 ng/mL	0.29 $\text{ng}/\text{g} \approx 2.7 \text{nmol}/\text{mL}$	This work

SLT surface using an electrochemical method, followed by anchoring AgNPs on the PPy@PEDOT:PSS film surface through self-assembly and electrochemical deposition method to form a AgNP/PPy@PEDOT:PSS/SLT sensor electrode. The CV curves and EIS spectra of the AgNP/PPy@PEDOT:PSS/SLT electrode demonstrated excellent electrochemical catalytic activity. The AgNP/PPy@PEDOT:PSS/SLT electrode was employed for SHF detection in milk and rice flour samples. The results showed an excellent linear relationship between SHF concentration and the peak of DPV current (relative to PBS background solution) in the 1–130 ng/mL range for the milk and rice flour samples. Furthermore, the LOD values for the EC sensor based on AgNP/PPy@PEDOT:PSS/SLT electrode were 0.58 and 0.29 ng/mL for SHF in milk and rice flour samples, respectively. Raman spectroscopy revealed the EC oxidization of SHF to formaldehyde. Therefore, the proposed AgNP/PPy@PEDOT:PSS/SLT electrochemical sensor holds significant potential for widespread use in food safety applications.

CRediT authorship contribution statement

Tianwen Xu: Conceptualization, Methodology, Writing – original draft. **Li Yang:** Investigation, Resources. **Xin Zhang:** Data curation. **Guo Lu:** Visualization. **Zhongchen Bai:** Writing – review & editing, Supervision, Project administration, Funding acquisition.

Declaration of Competing Interest

The authors declare that they have no known competing financial interests or personal relationships that could have appeared to influence the work reported in this paper.

Data availability

Data will be made available on request.

Acknowledgments

These works were supported by the National Natural Science Foundation of China (NSFC) (62065002, 61865002); The authors have declared that no conflicting interests exist.

Appendix A. Supplementary data

Supplementary data to this article can be found online at <https://doi.org/10.1016/j.fochx.2023.100701>.

References

- Abedalwafa, M. A., Tang, Z., Qiao, Y., Mei, Q., Yang, G., Li, Y., & Wang, L. J. M. A. (2020). An aptasensor strip-based colorimetric determination method for kanamycin using cellulose acetate nanofibers decorated DNA–gold nanoparticle bioconjugates. *Microchimica Acta*, 187, 1–9. <https://doi.org/10.1007/s00604-020-04348-x>
- Bavandpour, R., Karimi-Maleh, H., Asif, M., Gupta, V. K., Atar, N., & Abbasghorbani, M. J. J. (2016). Liquid phase determination of adrenaline uses a voltammetric sensor employing CuFe₂O₄ nanoparticles and room temperature ionic liquids. *Journal of Molecular Liquids*, 213, 369–373. <https://doi.org/10.1016/j.molliq.2015.07.054>
- Chapman, E., Barinaga, C., Udseth, H., & Smith, R. (1990). Confirmation and quantitation of hydroxymethanesulfonate in precipitation by electrospray ionization-tandem mass spectrometry. *Atmospheric Environment Part A. General Topics*, 24(12), 2951–2957. [https://doi.org/10.1016/0960-1686\(90\)90475-3](https://doi.org/10.1016/0960-1686(90)90475-3)
- Dong, Q., Ryu, H., & Lei, Y. J. E. A. (2021). Metal oxide based non-enzymatic electrochemical sensors for glucose detection. *Electrochimica Acta*, 370, Article 137744. <https://doi.org/10.1016/j.electacta.2021.137744>
- Dovrou, E., Lim, C. Y., Canagaratna, M. R., Kroll, J. H., Worsnop, D. R., & Keutsch, F. N. (2019). Measurement techniques for identifying and quantifying hydroxymethanesulfonate (HMS) in an aqueous matrix and particulate matter using aerosol mass spectrometry and ion chromatography. *Atmospheric Measurement Techniques*, 12(10), 5303–5315. <https://doi.org/10.5194/amt-12-5303-2019>
- Hatamluyi, B., & Es' hagh, Z. (2018). Electrochemical biosensing platform based on molecularly imprinted polymer reinforced by ZnO–graphene capped quantum dots for 6-mercaptopurine detection. *Journal of Pharmaceutical and Biomedical Analysis*, 283, 1170–1177. <https://doi.org/10.1016/j.jpba.2018.08.004>
- Jing, L., Li, J., Qin, M., Song, Y., Zhang, J., & Chen, Q. (2018). Development and characterization of sandwich-type enzyme-linked aptamer assay for the detection of rongalite in food. *Analytical Biochemistry*, 563, 25–34. <https://doi.org/10.1016/j.ab.2018.09.019>
- Jodan, I., Wantala, K., Amini, N., Shahmoradi, B., Ghaslani, M., & Lee, S.-M. (2020). Fabrication of a sensitive electrochemical sensor based on Ag nanoparticles and alizarin yellow polymer: Application to the detection of an environmental pollutant thiourea. *Korean Journal of Chemical Engineering*, 37, 1609–1615. <https://doi.org/10.1007/s11814-020-0561-y>
- Kaur, H., Sheoran, K., Siwal, S. S., Saini, R. V., Saini, A. K., Alsanie, W. F., & Thakur, V. K. J. M. (2022). Role of silver nanoparticle-doped 2-aminodiphenylamine polymeric material in the detection of dopamine (DA) with uric acid interference. *Materials*, 15(4), 1308. <https://doi.org/10.3390/ma15041308>
- Lebrun, N., Dhameincourt, P., Focsa, C., Chazallon, B., Destombes, J., & Prevost, D. J. J. (2003). Raman analysis of formaldehyde aqueous solutions as a function of concentration. *Journal of Raman Spectroscopy*, 34(6), 459–464. <https://doi.org/10.1002/jrs.1025>
- Li, Y., Xie, M., Zhang, X., Liu, Q., Lin, D., Xu, C., ... Chemical, A. B. (2019). Co-MOF nanosheet array: A high-performance electrochemical sensor for non-enzymatic glucose detection. *Sensors and Actuators B: Chemical*, 278, 126–132. <https://doi.org/10.1016/j.snb.2018.09.076>
- Liu, W., Bai, H., Li, X., Li, W., Zhai, J., & Li, J. (2018). Improved surface-enhanced Raman spectroscopy sensitivity on metallic tungsten oxide by the synergistic effect of surface plasmon resonance coupling and charge transfer. *The Journal of Physical Chemistry Letters*, 9(14), 4096–4100. <https://doi.org/10.1021/acs.jpcclett.8b01624>
- Loiseau, A., Zhang, L., Hu, D., Salmain, M., Mazouzi, Y., & Flack, R. (2019). Core-shell gold/silver nanoparticles for localized surface Plasmon resonance-based naked-eye toxin biosensing. *ACS Applied Materials & Interfaces*, 11(50), 46462–46471. <https://doi.org/10.1021/acsami.9b14980>
- Manikandan, V. S., Adhikari, B., & Chen, A. J. A. (2018). Nanomaterial based electrochemical sensors for the safety and quality control of food and beverages. *The Analyst*, 143(19), 4537–4554. <https://doi.org/10.1039/C8AN00497H>
- Maruno, S. J. O. E. (2019). Surface plasmon spectroscopy of thin composite films of Au nanoparticles and PEDOT: PSS conjugated polymer. *The Analyst*, 64, 154–157. <https://doi.org/10.1039/C8AN00497H>
- Mohan, A. V., Rajendran, V., Mishra, R. K., & Jayaraman, M. J. T. T. (2020). Recent advances and perspectives in sweat based wearable electrochemical sensors. *TrAC Trends in Analytical Chemistry*, 131, Article 116024. <https://doi.org/10.1016/j.trac.2020.116024>
- Nesměrák, K., Kudláček, K., Štícha, M., Kozlík, P., & Babica, J. J. M. (2019). HPLC-MS/MS analysis of degradation products of neosalvarsan in a 76-year-old injection preparation. *Monatshfte für Chemie - Chemical Monthly*, 150, 1611–1615. <https://doi.org/10.1007/s00706-019-02450-2>
- Noori, J. S., Mortensen, J., & Geto, A. J. S. (2020). Recent development on the electrochemical detection of selected pesticides: A focused review. *Sensors*, 20(8), 2221. <https://doi.org/10.3390/s20082221>
- Pasupuleti, K. S., Reddeppa, M., Park, B.-G., Peta, K. R., Oh, J.-E., & Kim, S.-G. (2020). Ag nanowire-plasmonic-assisted charge separation in hybrid heterojunctions of Ppy-PEDOT: PSS/GaN nanorods for enhanced UV photodetection. *ACS Applied Materials & Interfaces*, 12(48), 54181–54190. <https://doi.org/10.1021/acsami.0c16795>
- Qian, L., Durairaj, S., Prins, S., & Chen, A. J. B. (2021). Nanomaterial-based electrochemical sensors and biosensors for the detection of pharmaceutical compounds. *Biosensors and Bioelectronics*, 175, Article 112836. <https://doi.org/10.1016/j.bios.2020.112836>
- Ren, X., Yang, M., Yang, T., Xu, C., Ye, Y., & Wu, X. (2021). Highly conductive PPy-PEDOT: PSS hybrid hydrogel with superior biocompatibility for bioelectronics application. *ACS Applied Materials & Interfaces*, 13(21), 25374–25382. <https://doi.org/10.1021/acsami.1c04432>

- Shahmiri, M. R., Bahari, A., Karimi-Maleh, H., Hosseinzadeh, R., Mirnia, N. J. S., & Chemical, A. B. (2013). Ethynylferrocene-NiO/MWCNT nanocomposite modified carbon paste electrode as a novel voltammetric sensor for simultaneous determination of glutathione and acetaminophen. *Sensors and Actuators B: Chemical*, *177*, 70–77. <https://doi.org/10.1016/j.snb.2012.10.098>
- Song, D., Wang, Y., Lu, X., Gao, Y., Li, Y., Gao, F. J. S., & Chemical, A. B. (2018). Ag nanoparticles-decorated nitrogen-fluorine co-doped monolayer MoS₂ nanosheet for highly sensitive electrochemical sensing of organophosphorus pesticides. *Sensors and Actuators B: Chemical*, *267*, 5–13. <https://doi.org/10.1016/j.snb.2018.04.016>
- Tufa, L. T., Oh, S., Kim, J., Jeong, K.-J., Park, T. J., Kim, H.-J., & Lee, J. J. E. A. (2018). Electrochemical immunosensor using nanotriplex of graphene quantum dots, Fe₃O₄, and Ag nanoparticles for tuberculosis. *Electrochimica Acta*, *290*, 369–377. <https://doi.org/10.1016/j.electacta.2018.09.108>
- Wan, Y., Zheng, Y. F., Wan, H. T., Yin, H. Y., & Song, X. C. J. F. C. (2017). A novel electrochemical sensor based on Ag nanoparticles decorated multi-walled carbon nanotubes for applied determination of nitrite. *Food Control*, *73*, 1507–1513. <https://doi.org/10.1016/j.foodcont.2016.11.014>
- Wang, J., Zheng, W., Zhang, Y., Song, S., Chou, I.-M., Hu, M., & Pan, Z. J. C. (2020). Raman spectroscopic technique towards understanding the degradation of phenol by sodium persulfate in hot compressed water. *Chemosphere*, *257*, Article 127264. <https://doi.org/10.1016/j.chemosphere.2020.127264>
- Wang, X., Jiang, J., Zhang, Q., & Bai, Z. J. O. M. (2021). The high active SERs substrate prepared by self assembling Ag nanoparticles on PPy@ PEDOT: PSS film to detect the sodium formaldehyde sulfoxylate molecules. *Optical Materials*, *114*, Article 110955. <https://doi.org/10.1016/j.optmat.2021.110955>
- Wang, X., Lu, A., Bai, Z., & Xu, T. J. A. (2022). A multilayer interlaced Ag nanosheet film prepared by an electrodeposition method on a PPy@ PEDOT: PSS film: A strategy to prepare sensitive surface-enhanced raman scattering substrates. *ACS Omega*, *7*(11), 9380–9387. <https://doi.org/10.1021/acsomega.1c06387>
- Wang, Y., Yan, L., Cheng, R., Muhtar, M., Shan, X., & Xiang, Y. (2018). Multifunctional HA/Cu nano-coatings on titanium using PPy coordination and doping via pulse electrochemical polymerization. *Biomaterials Science*, *6*(3), 575–585. <https://doi.org/10.1039/C7BM01104K>
- Wei, L., Fu, P., Chen, X., An, N., Yue, S., Ren, H., ... Letters, T. (2020). Quantitative determination of hydroxymethanesulfonate (HMS) using ion chromatography and UHPLC-LTQ-orbitrap mass spectrometry: A missing source of sulfur during haze episodes in Beijing. *Environmental Science & Technology Letters*, *7*(10), 701–707. <https://doi.org/10.1021/acs.estlett.0c00528>
- Wu, Y., Wang, X., Wen, X., Zhu, J., Bai, X., Jia, T., ... Qi, Y. J. P. L. A. (2020). Surface-enhanced Raman scattering based on hybrid surface plasmon excited by Au nanodisk and Au film coupling structure. *Physics Letters A*, *384*(23), Article 126544. <https://doi.org/10.1016/j.physleta.2020.126544>
- Wu, Z., Guo, F., Huang, L., & Wang, L. J. F. (2018). Electrochemical nonenzymatic sensor based on cetyltrimethylammonium bromide and chitosan functionalized carbon nanotube modified glassy carbon electrode for the determination of hydroxymethanesulfonate in the presence of sulfite in foods. *Food Chemistry*, *259*, 213–218. <https://doi.org/10.1016/j.foodchem.2018.03.080>
- Xia, Y., & Ouyang, J. J. A. (2010). Significant conductivity enhancement of conductive poly (3, 4-ethylenedioxythiophene): Poly (styrenesulfonate) films through a treatment with organic carboxylic acids and inorganic acids. *ACS Applied Materials & Interfaces*, *2*(2), 474–483. <https://doi.org/10.1021/am900708x>
- Xiao, T., Huang, J., Wang, D., Meng, T., & Yang, X. J. T. (2020). Au and Au-Based nanomaterials: Synthesis and recent progress in electrochemical sensor applications. *Talanta*, *206*, Article 120210. <https://doi.org/10.1016/j.talanta.2019.120210>
- Xiong, S., Zhou, J., Wu, J., Li, H., Zhao, W., He, C., ... Duan, H. (2021). High performance acoustic wave nitrogen dioxide sensor with ultraviolet activated 3D porous architecture of Ag-decorated reduced graphene oxide and polypyrrole aerogel. *ACS Applied Materials & Interfaces*, *13*(35), 42094–42103. <https://doi.org/10.1021/acscami.1c13309>
- Yola, M. L., Atar, N., Eren, T., Karimi-Maleh, H., & Wang, S. J. R. (2015). Correction: Sensitive and selective determination of aqueous triclosan based on gold nanoparticles on polyoxometalate/reduced graphene oxide nanohybrid. *RSC Advances*, *5*(89), 72590–72591. <https://doi.org/10.1039/C5RA90080H>
- Yuan, W., Xiang, B., Yu, L., & Xu, J. J. F. A. M. (2011). A non-invasive method for screening sodium hydroxymethanesulfonate in wheat flour by near-infrared spectroscopy. *Food Analytical Methods*, *4*, 550–558. <https://doi.org/10.1007/s12161-011-9198-0>
- Yue, G., Wu, J., Xiao, Y., Lin, J., Huang, M., & Lan, Z. J. T. J. (2012). Application of poly (3, 4-ethylenedioxythiophene): Polystyrenesulfonate/polypyrrole counter electrode for dye-sensitized solar cells. *The Journal of Physical Chemistry C*, *116*(34), 18057–18063. <https://doi.org/10.1021/jp303958r>
- Zahed, F. M., Hatamluyi, B., Lorestani, F., & Es'haghi, Z. (2018). Silver nanoparticles decorated polyaniline nanocomposite based electrochemical sensor for the determination of anticancer drug 5-fluorouracil. *Journal of Pharmaceutical and Biomedical Analysis*, *161*, 12–19. <https://doi.org/10.1016/j.jpba.2018.08.004>
- Zhang, X., Zhang, B., Ouyang, X., Chen, L., & Wu, H. J. T. J. (2017). Polymer solar cells employing water-soluble polypyrrole nanoparticles as dopants of PEDOT: PSS with enhanced efficiency and stability. *The Journal of Physical Chemistry C*, *121*(34), 18378–18384. <https://doi.org/10.1021/acs.jpcc.7b05767>
- Zhu, A., Gao, R., Zhao, X., Zhang, F., Zhang, X., Yang, J., ... Wang, Y. J. N. (2019). Site-selective growth of Ag nanoparticles controlled by localized surface plasmon resonance of nanobowl arrays. *Nanoscale*, *11*(14), 6576–6583. <https://doi.org/10.1039/C8NR10277E>
- Zuo, Y., & Chen, H. J. T. (2003). Simultaneous determination of sulfite, sulfate, and hydroxymethanesulfonate in atmospheric waters by ion-pair HPLC technique. *Talanta*, *59*(5), 875–881. [https://doi.org/10.1016/S0039-9140\(02\)00647-1](https://doi.org/10.1016/S0039-9140(02)00647-1)